Magnetic Resonance in Medicine 42:1004–1010 (1999)

The Relationship Between the BOLD-Induced T_2 and T_2^*: A Theoretical Approach for the Vasculature of Myocardium

Wolfgang R. Bauer,[1]* Walter Nadler,[2] Michael Bock, Lothar R. Schad,[3] Christian Wacker,[3] Andreas Hartlep,[3] and Georg Ertl[1]

Recently the blood oxygenation level–dependent (BOLD)-related T_2^* of myocardium was derived as an analytical function of intracapillary blood volume, blood oxygenation, and nuclear spin diffusion. The basis of this approach was to approximate the diffusion-induced field fluctuations a nuclear spin is subjected to by strong collision dynamics, i.e., the field fluctuations are uncorrelated. The same analysis is now performed for spin echo experiments that gives myocardial T_2 as a function of the parameters above and the echotime. An analytical relationship between T_2 and T_2^* relaxation is derived. The dependence of T_2 on diffusion, echo time, and blood oxygenation is congruent with simulation and experimental data. Magn Reson Med 42: 1004–1010, 1999. © **1999 Wiley-Liss, Inc.**

Key words: BOLD; myocardial imaging; heart; T_2^*

We recently presented an analytical approach in which the blood oxygenation level–dependent (BOLD)-related transverse relaxation time T_2^* of a free induction decay (FID) was derived as a function of tissue parameters as relative intracapillary blood volume and intracapillary blood oxygenation (1). The vascular architecture analyzed was that of myocardium. The basis for this approach was the strong collision approximation of the dynamics of field fluctuations a nuclear spin is subjected to while diffusing in the inhomogeneous pericapillary magnetic field. We could demonstrate (1) that the model predicts data of simulations well (2), experiments in animals (3), and measurements in humans (4,5). In this paper we extend our model to spin echo experiments, i.e., the transverse relaxation time T_2 is derived as a function of tissue parameters and echo time. The analysis is performed for a single and a biexponential approximation of the FID. The results are compared with simulation experiments of Kennan et al. (2) and experimental data of Atalay et al. (3). Finally, a general relation between T_2^* and T_2 is derived.

TISSUE MODEL

The type of tissue model we used for our analysis was recently introduced by us (1). The only vessel type considered are capillaries, because of their dominating volume contribution [>90% vessel volume (6)] in myocardium. Capillaries are considered as parallel cylinders (radius R_c) with a regular intercapillary spacing. Instead of taking spin diffusion in the whole tissue into account, we only consider one capillary with its concentric supply area (radius R_s), which implies that the relative intracapillary volume fraction is $RBV = (R_c/R_s)^2$. This Krogh model implies the introduction of reflectory diffusive boundary conditions at R_s. Because the capillary wall is almost impermeable on the time scale of transverse spin relaxation (7) one assumes reflectory boundary conditions at R_c as well. Due to the length of the capillaries (>400 μm) spin diffusion in the magnetic field gradient parallel to the capillary axis does not contribute much to spin relaxation. Hence, it is sufficient to consider 2D spin diffusion between two concentric cylinders with radius R_c and R_s. We only consider the extravascular fraction of spins due to its dominating contribution [>90% (8)]. The percapillary magnetic field is induced by paramagnetic intracapillary hemoglobin. The precession frequency of this field around the capillary (cylindrical coordinates $x = (r, \phi)$) is determined according to basic magnetostatics as

$$\omega(r, \phi) = -\delta\omega \cdot R_c^2 \cos(2\phi)/r^2, \qquad [1]$$

with the characteristic equatorial frequency shift of a magnetized cylinder, $\delta\omega = |\omega(R_c, 0)| = 2\pi\gamma \cdot \Delta M$. The term $\Delta M = \Delta\chi \cdot B_0 \cdot \sin^2(\theta)$ is the difference of extra- and intracapillary magnetization (cgs units), which is induced in an external magnetic field B_0 due to the susceptibility difference $\Delta\chi$. θ is the angle between capillary axis and external field, which is assumed to be 90° throughout this paper.

MATHEMATICAL ANALYSIS

Free Induction Decay in the Strong Collision Approximation

We recently presented a theory (1) in which the BOLD-related FID is derived as a function of microcirculatory parameters in myocardium. The decisive step was to replace the diffusion-induced field fluctuations that influence a precessing nuclear spin, by a strong collision dynamics. This was justified, because the correlation time of these field fluctuations was much shorter than the

[1]II. Medizinische Universitätsklinik Mannheim/Heidelberg, Mannheim, Germany.

[2]HLRZ c/o Forschungszentrum Jülich, Jülich, Germany.

[3]Department of Biophysics, German Cancer Research Center, Heidelberg, Germany.

Grant sponsors: Deutsche Gesellschaft für Kardiologie; Forschungsfonds des Klinikum Mannheim/Heidelberg Projekt 42; Grant Sonderforschungsbereich 355 "Pathophysiologie der Herzinsuffizienz"; Graduiertenkolleg "NMR"; Grant number: HA 1232/8-1.

*Correspondence to: Dr. W.R. Bauer, Medizinische Universitätsklinik Würzburg, Josef Schneider Str. 2, 97080 Würzburg, Germany.

Received 27 May 1999; revised 26 August 1999; accepted 15 September 1999.

BOLD-related relaxation time. In this paper only essentials are repeated.

The time evolution of the local transverse nuclear magnetization (polar notation: $m = m_x - im_y$) is determined by the Bloch-Torrey equation (diffusion coefficient D)

$$\partial_t m(x,\ t) = (D\nabla^2 + i \cdot \omega(x))m(x, t), \qquad [2]$$

which, after formal time integration, provides

$$m(x, t) = \exp\,[(D\nabla^2 + i \cdot \omega(x)) \cdot t]m(x, 0), \qquad [3]$$

and for the mean magnetization in the tissue volume V

$$M(t) = \frac{1}{V}\int_V dx\, \exp\,[(D\nabla^2 + i \cdot \omega(x)) \cdot t]m(x, 0) \qquad [4]$$

The correlation time of field fluctuations a diffusing nuclear spin is subjected to is (1)

$$\tau = (R_c^2/4D) \cdot |\ln RBV|/(1 - RBV), \qquad [5]$$

for the tissue model considered above. This correlation time is smaller than 6 msec when realistic values for myocardial tissue are inserted ($RBV = 5 - 10\%$, $R_c = 2.75$ µm, $D = 1$ µm^2/msec), i.e., smaller than the myocardial relaxation time $T_2^* > 30$ msec, and, hence, much smaller than the BOLD-related contribution to T_2^*. This implies that on a time scale on which significant alterations of transverse magnetization occur, the magnetic field fluctuations are stochastically independent. Uncorrelated field fluctuations may be considered as a stationary Markov process the generator of which is

$$\mathbf{D} = \lambda(\mathbf{\Pi} - \mathbf{id}), \qquad [6]$$

(9,10) where $\mathbf{\Pi}$ denotes the projection operator onto the functional space generated by the probability density function of the steady state $p(x)$ of this dynamic process [in this case $p(x)$ is identical with the spin density function (1)], i.e., $\mathbf{\Pi}f(x) = p(x) \cdot \int_V dx\, f(x)$ and **id** denotes the identity operator. Such an approach is refered to as strong collision approach. The parameter λ is the fluctuation frequency. Self consistency of the strong collision approximation implies that $\lambda = \tau^{-1}$. Replacement of the diffusion operator $D\nabla^2$ in Eqs. [3] and [4] by the strong collision operator **D** allows the analytical determination of the Laplace transform $\hat{M}(s) = \int_0^\infty dt\, e^{-st}M(t)$ as

$$\hat{M}(s) = (1 + RBV) \cdot (\sqrt{(s + \tau^{-1})^2 + \delta\omega^2 RBV^2} + RBV\sqrt{(s + \tau^{-1})^2 + \delta\omega^2} - \tau^{-1}(1 + RBV))^{-1} \qquad [7]$$

The relaxation time of the free induction process is determined according to the mean relaxation time approximation [11] as $T_2^* = \hat{M}(0)$, i.e.,

$$T_2^* = \tau \cdot (1 + RBV) \cdot ([\sqrt{1 + (\tau\delta\omega \cdot RBV)^2} - 1] + RBV \cdot [\sqrt{1 + (\tau\delta\omega)^2} - 1])^{-1}, \qquad [8]$$

Spin Echoes in the Strong Collision Approximation

In this section we will derive the time course of the transverse magnetization, which is subjected to a spin echo sequence. It has to be stressed that the derived relations between reversible and irreversible spin dephasing only depend on the strong collision assumption and do not assume any special form of geometry or form of the inhomogeneous field. A simple spin echo sequence consists of a 90° pulse with a subsequent 180° pulse after $t/2$. The echo is gained after the echo time t.* After each pulse there is a simple free induction relaxation of the transverse magnetization, however, the phase reflection induced by the 180°-pulse refocuses coherent dephasing at t, i.e., the loss of transverse magnetization at t is due to incoherent, i.e., irreversible dephasing.

In the strong collision approximation the time evolution of the local magnetization at $t/2$ before the 180° pulse is given by

$$m(x, t/2) = \exp\,[\mathbf{G}t/2]m(x, 0), \qquad [9]$$

where we introduced the time evolution generator of the FID, $\mathbf{G} = \mathbf{D} + i \cdot \omega(x)$ (Eq. [6]). The 180° pulse induces a reflection of the phase which mathematically leads to a transition of $m(x, t/2)$ to its complex adjoint

$$m(x, t/2) \xrightarrow{180°\ \text{pulse}} m^*(x, t/2) = \exp\,[\mathbf{G}^*t/2]m^*(x, 0) \qquad [10]$$

After the 180° pulse time evolution is given by

$$m(x, t/2 + \Delta t) = \exp\,[\mathbf{G}\Delta t]\ m^*(x, t/2) = \exp\,[\mathbf{G}\Delta t]\exp\,[\mathbf{G}^*t/2]m^*(x, 0) \qquad [11]$$

and at the echo time t

$$m(x, t) = \exp\,[\mathbf{G}t/2]\exp\,[\mathbf{G}^*t/2]\mathbf{1} \qquad [12]$$

where we exploited that the initial magnetization is homogeneous and normalized to 1, i.e., $m(x, 0) = \mathbf{1}$, with the function $\mathbf{1} \equiv 1$.

*We denote the echo time as t instead of the commonly used TE to simplify the editing of the mathematical formulas.

The mean magnetization in the tissue volume V at the echo time is given by

$$M_{SE}(t) = \frac{1}{V}\int_V dV m(x, t)$$

$$= \frac{1}{V}\int_V dV \exp[\mathbf{G}t/2] \exp[\mathbf{G}^*t/2]\mathbf{1}. \quad [13]$$

Equations [12] and [13] and the structure of the operators **G** and **D** imply that

$$\frac{d}{dt} M_{SE}(t) = \frac{1}{V}\int_V dV \exp[\mathbf{G}t/2][\mathbf{G}/2 + \mathbf{G}^*/2] \exp[\mathbf{G}^*t/2]\mathbf{1}$$

$$= \frac{1}{V}\int_V dV \exp[\mathbf{G}t/2]\mathbf{D} \exp[\mathbf{G}^*t/2]\mathbf{1}$$

$$= \frac{1}{V}\int_V dV \exp[\mathbf{G}t/2]\frac{1}{\tau}(\mathbf{\Pi} - \mathbf{id}) \exp[\mathbf{G}^*t/2]\mathbf{1}$$

$$= \frac{1}{\tau}\frac{1}{V}\left(\int_V dV \exp[\mathbf{G}t/2]\mathbf{1}\right)\frac{1}{V}\left(\int_V dV \exp[\mathbf{G}^*t/2]\mathbf{1}\right)$$

$$- \frac{1}{\tau}\frac{1}{V}\left(\int_V dV \exp[\mathbf{G}t/2] \exp[\mathbf{G}^*t/2]\mathbf{1}\right)$$

$$= \frac{1}{\tau} M(t/2) \cdot M^*(t/2) - \frac{1}{\tau} M_{SE}(t)$$

$$= \frac{1}{\tau}|M(t/2)|^2 - \frac{1}{\tau} M_{SE}(t), \quad [14]$$

where the function $M(t)$ denotes the time course of magnetization during the free induction decay. Equation [14] is a simple first order differential equation which is solved by

$$M_{SE}(t) = e^{-t/\tau} + e^{-t/\tau}\frac{1}{\tau}\int_0^t d\xi e^{\xi/\tau}|M(\xi/2)|^2 \quad [15]$$

Equation [15] defines the exact time course of magnetization $M_{SE}(t)$ after the echo time t when the strong collision model is assumed. The determination of T_2 from Eq. [15] requires the knowledge of the free induction decay of magnetization $M(t)$. When a single exponential decay of the FID is assumed, i.e., $M(t) \approx e^{-R_2^* t}$, Eq. [15] becomes

$$M_{SE}(t) = e^{-t/\tau} + e^{-t/\tau}\frac{1}{\tau}\int_0^t d\xi e^{\xi/\tau} e^{-R_2^*\xi}$$

$$= e^{-t/\tau} + e^{-t/\tau}\frac{1}{1 - \tau R_2^*}(e^{(1/\tau - R_2^*)t} - 1)$$

$$= \frac{\tau}{1 - \tau R_2^*}(\tau^{-1}e^{-R_2^* t} - R_2^* e^{-t/\tau}) \quad [16]$$

When a biexponential FID is assumed, i.e., $M(t) = f_1 e^{-\Gamma_1 t} + f_2 e^{-\Gamma_2 t}$ (for the derivation of f_i and Γ_i see Appendix), Eq. [15] provides M_{SE} as

$$M_{SE}(t) = e^{-t/\tau}(1 + C_1 + C_2 + C_3), \quad [17]$$

with

$$C_1 = \frac{f_1^2}{1 - \tau\Gamma_1}(e^{(1/\tau - \Gamma_1)t} - 1) \quad [18]$$

$$C_2 = \frac{f_2^2}{1 - \tau\Gamma_2}(e^{(1/\tau - \Gamma_2)t} - 1) \quad [19]$$

$$C_3 = \frac{2f_1 f_2}{1 - \tau\Gamma}(e^{(1/\tau - \Gamma)t} - 1), \quad [20]$$

where $\Gamma = (\Gamma_1 + \Gamma_2)/2$.

APPLICATIONS

Relaxation Rate and Echo Time

When T_2 or the corresponding rate R_2 is determined from a spin echo (multiecho) experiment one assumes a single exponential decay of the magnetization $M_{SE} \approx e^{-t R_2}$ at the echo time (or between two echoes at the interechotime) t, which leads to (see Eq. [15])

$$R_2 = \frac{-\ln M_{SE}(t)}{t} \quad [21]$$

Figure 1 demonstrates for different diffusion coefficients the relaxation rate R_2 determined from Eq. [21] as a function of the echo time. A single exponential and a biexponential approximation of the FID in Eq. [15] is analyzed (Eqs. [16] and [17]). One obtains that with increasing echo time the relaxation rate becomes independent from echo time and that this asymptotic value is the same for the single and biexponential FID approximation. Increasing the diffusion coefficient makes this relation evident for shorter echo times. At short echo times the rates are considerably smaller when a biexponential FID is assumed and these data agree better with simulation experiments.

The explanation is given in Fig. 2, where the magnetization decay (Eq. [15]) at the echo time was determined either for a bi- or a single exponential FID approximation in Eq. [15] for two diffusion regimes. For long echo times the magnetization-echo time curves are almost identical for both approximations. However, when short echo times or interecho times are considered there is a considerable difference (Fig. 2b). In the short echo time range ($1 - M_{SE}(t) \ll 1$) the relaxation rate determined from Eq. [21] may be approximated as $R_2 = -\ln M_{SE}(t)/t \approx (1 - M_{SE}(t))/t$, i.e., Fig. 2b demonstrates that R_2 obtained from a single or a biexponential FID differs by more than 100%. This and the comparison with simulation data (Fig. 1) implies that the determination of the transverse relaxation rate requires a biexponential approximation of the FID when short (inter-) echo times are considered.

Comparison With Simulations of Kennan et al.

Kennan et al. (2) determined R_2^* and R_2 from simulations of spins diffusing within a quadratic box containing a vessel inside, which was filled with a paramagnetic contrast agent. The orientation of the vessel axis was perpendicular to the external field ($\theta = 90°$) and the length of the box was that of the intercapillary distance. The rate R_2^* was determined from a FID and R_2 from spin echo (multi echo) experiments with varying echo time. We could recently demonstrate that our analytical model (1) predicted well the R_2^* data of FID simulations. In this section we will compare the predictions of our model with the simulations of spin echo experiments.

In one part of his study, Kennan et al. considered R_2 and R_2^* as a function of the diffusion coefficient. When $M_{SE}(t)$ is determined according to Eq. [16], i.e., we assume a single exponential decay of the FID ($M(t)$), the calculated data of R_2 (Eq. [21]) are in close congruence with the simulation data (Fig. 3). The dependence of R_2 on the echotime is also well reflected. The simulation data and our results demonstrate similar characteristic features of the dependence of R_2 on the diffusion coefficient.

- there is a single maximum
- with increasing diffusion coefficient (small correlation times) R_2 becomes independent from the echo time
- $R_2 \approx R_2^*$ when the diffusion coefficient increases. This is the the motional narrowing limit ($\tau \rightarrow 0$), i.e., $R_2 \approx R_2^* \approx \tau \cdot RBV \cdot \delta\omega^2/2$ (Eq. [8], Fig. 3 and Ref. 1).

In another set of simulations Kennan et al. considered the dependence $R_2(D)$ for different vessel sizes (Fig. 4).

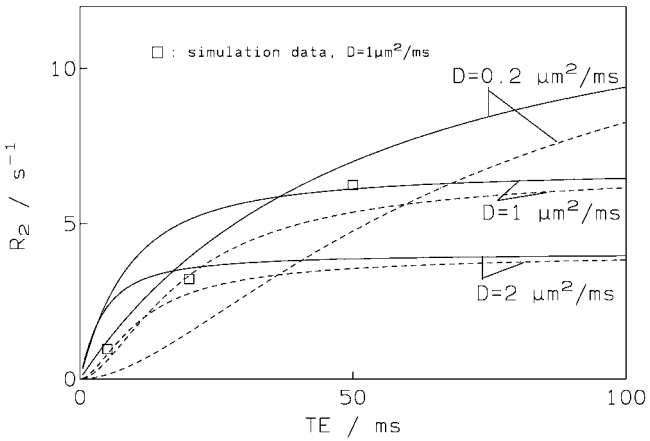

FIG. 1. Transverse relaxation rate R_2 as a function the echo time TE obtained from Eq. [21] and Eqs. [15], [16], and [17]. The difference between intra- and extracapillary magnetization ($=\Delta\chi \cdot B_0$) was assumed to be 1.6 mgauss, which is the valid for deoxygenated blood ($\Delta\chi = 8 \cdot 10^{-8}$ for hematocrit = 40%) in an external field of $B_0 = 2$T. A single (solid line) and a biexponential (dashed line) approximation of the FID is inserted in Eq. [15]. Three different diffusion regimes (coefficient D) are considered for a relative intracapillary blood volume $RBV = 5\%$ and a capillary radius $R_c = 2.5$ μm. The squares denote relaxation rates of simulated spin-echo experiments ($D = 1$ μm²/ms, $RBV = 5\%$) for different echotimes (TE = 50, 20, 5 msec) and are taken from Ref. 2. Note that for short echo times, the predictions of the model are closer to simulation data when a biexponential decay of the FID is assumed.

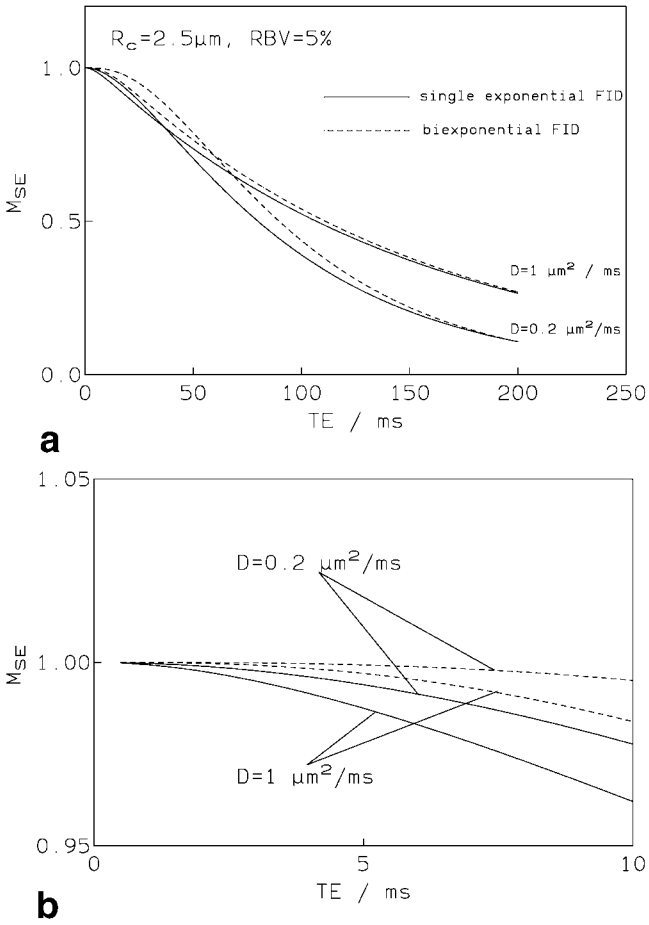

FIG. 2. **a**, **b:** Magnetization M_{SE} as a function of the echo time TE according to Eq. [15] for two different diffusion regimes. As in Fig. 1 a single (solid line) and a biexponential (dashed line) FID approximation is inserted in Eq. [15]. **b**: a magnification of **a** for the range of short echo times.

When R_2 is determined according to Eq. [21] there is again a close congruence between data obtained from simulations and those predicted by our model. The increase of the vessel size leads to a shift of the $R_2(D)$ curve to the right, which is explained by the increase of the correlation time (Eq. [5]).

Comparison With Experimental Data

Atalay et al. determined T_2^* (12) and T_2 (3) in isolated rabbit hearts that were perfused with a red cell suspension at various oxygenation levels. Because experiments were performed under cardioplegic conditions and after maximal vasodilation the oxygenation gradient along the capillary axis was negligible as was recently estimated by us (1). This implies that the intracapillary oxygenation of hemoglobin is almost that of the perfusate. The authors found empirical equations for the dependence of R_2^* and R_2 on the relative oxygen saturation of hemoglobin Y as demonstrated in Fig. 5. The experimental setup of the horizontal imaging system and the heart preparation (12) suggests an almost perpendicular intersection of the capillary axis and the external field. For comparison with our theory we determined R_2^* from Eq. [8] and R_2 from Eq. [21]. The equatorial frequency shift $\delta\omega$ (Eqs. [1] and [8]) was deter-

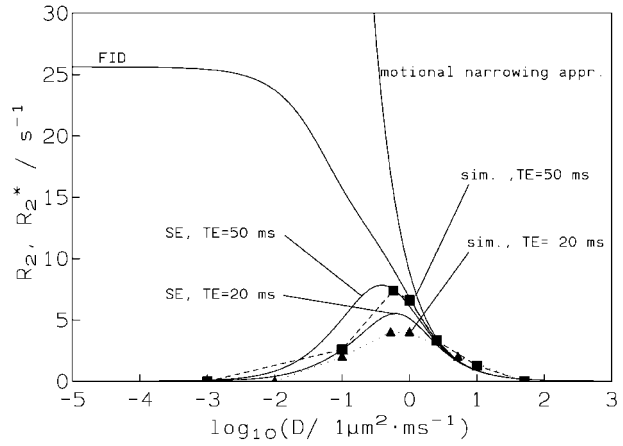

FIG. 3. Relaxation rate as function of the diffusion coefficient *D* for a free induction decay (R_2^*, FID) and spin-echo experiments (R_2, SE). For comparison with simulation data, the tissue parameters were taken from Ref. 2 as: relative intracapillary blood volume *RBV* = 5%, capillary radius R_c = 2.5 μm, intracapillary magnetization of 1.6 mG ($\delta\omega$ = 269 rad · sec^{-1}). The data from the model (solid lines) were obtained from Eq. [8] (FID) and Eqs. [16] and [21] (spin echo). Two echo times were analyzed and compared with simulation curves (square/triangle: spin-echo simulation data for an echo time of 50/20 msec). Note that with increasing diffusion coefficient (decreasing correlation time) both, the relaxation rate of the FID and those of the spin-echo experiments approach the motional narrowing limit, i.e., $R_2 \approx R_2^* \approx \tau \cdot RBV \cdot \delta\omega^2/2$.

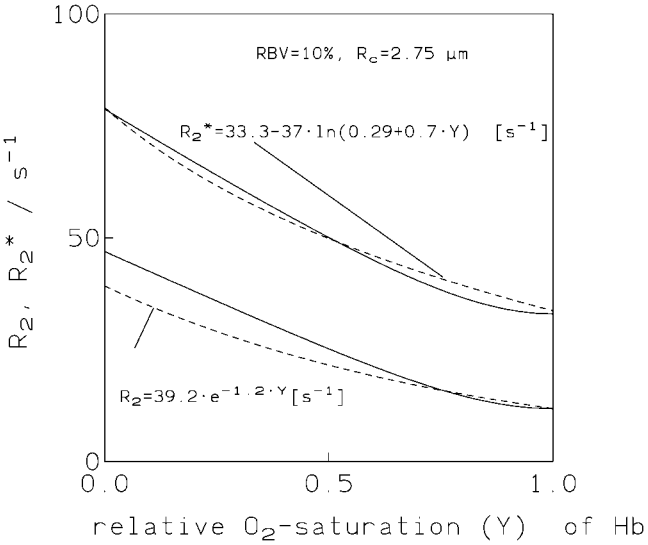

FIG. 5. Myocardial R_2^* and R_2 as a function of the relative oxygen saturation of hemoglobin *Y*. The dashed curves were obtained from empirical equations that Atalay et al. (3) found in red cell–perfused rabbit hearts at 4.7 T from gradient-echo and spin-echo experiments. The solid curves were obtained from Eq. [8] ($R_2^*(Y)$) and Eqs. [16] and [21] ($R_2(Y)$). The relative intracapillary blood volume was assumed to be 10%, which is reasonable for a dilated microvascular system (8), and the capillary radius was assumed to be 2 75 μm, which is a realistic value for a capillary in myocardium (13). Note the congruence between the empirical curves and those obtained from the model.

mined as $\delta\omega = 2\pi\gamma \cdot \Delta\chi_0(1 - Y) \cdot B_0$ where γ denotes the gyromagnetic ratio, $\Delta\chi_0 = 8 \cdot 10^{-8}$ is the susceptibility difference for complete deoxygenated blood ($Y = 0$), and B_0 = 4.7 T is the external magnetic field. Because the authors state that the relaxation rate R_2 was independent from echotime (range: 18–1000 msec) when determined according to Eq. [21] it is justified to describe the magnetization decay $M_{SE}(t)$ by Eq. [16] (Fig. 1). Because Atalay et al. only gave the range of echotimes they used in their experiments we assumed an echotime of 23 msec that appears to be reasonable to detect also fast relaxation in the presence of low blood oxygenation. The relative intracapillary blood volume (RBV) was assumed to be 10%, which is a realistic value for a dilated microvascular system (8). Because our theory describes the BOLD-related part of transverse relaxation, the offset of the empirical curves at 100% oxygen saturation ($R_2^*(Y = 1)$, $R_2(Y = 1)$) was added to our theoretical curves. As the empirical curves, the $R_2^*(Y)$ and $R_2(Y)$ curves obtained from our model almost run parallel (Fig. 5), and there is evident similarity between the empirical and analytical function.

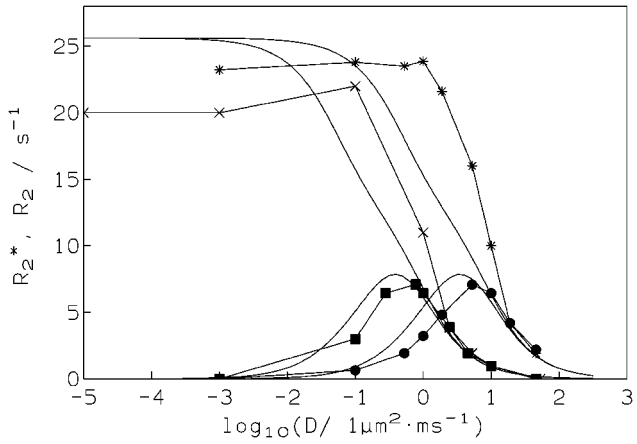

FIG. 4. Relaxation rates of free induction decay (R_2^*) and spin-echo experiments (R_2, echo time TE = 50 msec). The capillary radius is 2.5 μm (X, gradient echo; square, spin-echo simulation data) and 7.5 μm (*, gradient echo; circle, spin-echo simulation data). Solid lines are obtained from the model.

General Relation Between Irreversible and Reversible Spin Dephasing and Correlation Time

In this section we will derive a general relation between T_2 and T_2^* when the strong collision approach is applied. In this section above the relaxation time (rate) was determined from a single echo time *t* or interecho time when a multiecho sequence is applied. From a more theoretical point of view T_2 should be obtained from a signal echo time curve, i.e., many single spin-echo experiments with different echotimes are required. In this case one cannot apply Eq. [21] for determination of the transverse relaxation time (rate). Instead the best single exponential approximation of magnetization decay is required $M_{SE}(t) \approx e^{-t/T_2}$, which according to the mean relaxation time approximation (11) is

$$T_2 = \int_0^\infty dt\, M_{SE}(t), \qquad [22]$$

Insertion of $M_{SE}(t)$ from Eq. [15] gives

$$T_2 = \int_0^\infty dt\, e^{-t/\tau} + \int_0^\infty dt e^{-t/\tau}\left(\frac{1}{\tau}\int_0^t d\xi e^{\xi/\tau}|M(\xi/2)|^2\right)$$

$$= \tau + 2 \cdot |\hat{M}|^2(0), \qquad [23]$$

where we applied the integration, translation, and similarity theorem of Laplace transforms. The further evaluation depends on the approximation of the FID, i.e., $M(t)$. When we assume a single exponential decay, i.e., $M(t) \approx e^{-t/T_2*}$ we obtain

$$T_2 \approx \tau + T_2^*, \qquad [24]$$

that reveals a very simple relationship between T_2 and T_2^*. It has to be stated the derivation of the relation 24 is based on the single exponential form of the FID of tranverse magnetization M. This appears to be a reasonable assumption as long as the T_2 relaxation is obtained from long echotimes. However, when T_2 is obtained from measurements at short echotimes a more precise description of the FID is necessary.

The relation 24 reveals some fundamental properties between T_2 and T_2^*. In the limit of very long correlation times $\tau \rightarrow \infty$ (static dephasing regime) one obtains

$$T_2 \gg T_2^* \qquad [25]$$

which reflects the fact that in this limit there is only a minor portion of irreversible dephasing of transversal polarized spins. In the opposite case, i.e., $\tau \rightarrow 0$ (motional narrowing limit) the relation 24 becomes

$$T_2 \approx T_2^* \qquad [26]$$

i.e., the most part of dephasing is irreversible.

DISCUSSION

In this paper we demonstrated that our analysis of BOLD-related transverse relaxation can be extended from the free induction decay to spin-echo experiments. A general relation between irreversible and reversible spin dephasing was obtained.

Strong Collision Approach

The base of our analysis is the strong collision approach of the dynamics of the BOLD-related field fluctuations, which is justified according to the relation of correlation and relaxation time ($\tau \ll T_{2,BOLD}*$) in myocardium. The interval of correlation times, which satisfy the strong collision condition contains that for which the motional narrowing condition $\tau \cdot \sqrt{\langle \Delta\omega^2 \rangle} \ll 1$ is valid ($\langle \Delta\omega^2 \rangle$ = variance of field fluctuations) because in this limit $R_2^* = \tau \cdot \langle \Delta\omega^2 \rangle$, i.e. $R_2{*}\tau \ll 1$. The opposite, however, is not true as was recently demonstrated (1).

Furthermore the model presented here also contains the static dephasing regime of spin relaxation as a special case, because static dephasing is the asymptotic state of both dynamics, the diffusion and the strong collision generated field fluctuations. This implies that the strong collision approach represents a two side approximation of spin relaxation. It interpolates relaxation rates coming from very long (static dephasing regime) and short ($\tau \ll T_{2,BOLD}$) correlation times.

Kiselev and Posse (14,15) recently presented analytical models to describe transverse relaxation for very long and short correlation times. The first extends the static dephasing regime by consideration of spin diffusion within a local linear field gradient (14,15). The other model, which is used for the description of the fast motion regime, is a perturbation approach in the local magnetic fields (14). The data provided by these models are very close to simulation data of Boxerman et al. (16). The vascular network Kiselev and Posse focused on was that of the brain. This implies that the BOLD effect around larger vessels (veins) has to be considered, i.e., approximations near the static dephasing regime are important. In myocardium, however, the relative volume of the venous system is negligible (6). On the other hand, we have recently shown (1) that the motional narrowing condition is not fulfilled in the capillary system of myocardium which hampers the application of perturbation approaches. One of our future goals is to apply our model to a cerebrovascular network and to compare our analytical results with those of Kiselev and Posse.

Determination of Relaxation Time

We could derive simple relations for the relaxation time or rate as a function of the echo time. It could be demonstrated that for very short echo times (interecho times) a biexponential approximation of the FID leads to rates, which are closer to simulation data.

A general relation between T_2 and T_2^* was obtained under the assumption that T_2 is obtained from a signal (magnetization) echo time curve. It has to be stressed that the simple relation 24 is only valid for the BOLD-related part of transverse relaxation, i.e., relaxation is induced by field fluctuations with a single correlation time. However, in tissue spin dephasing is induced by field fluctations, the dynamics of which is a result of a complex superposition of single processes having their own correlation times.

APPENDIX: BIEXPONENTIAL APPROXIMATION OF THE T_2^* RELAXATION

The generalized moment expansion represents an algorithm to approximate a relaxation time curve $M(t)$ by a sum of exponentials (10,11), $M(t) \approx \Sigma_{\nu=1}^{N} f_\nu \cdot \exp(-t\Gamma_\nu)$. The function and its approximation have the same statistical moments. High-frequency moments describe the short time behavior and are the jets of the Taylor expansion of $M(t)$, i.e., $\mu_n = M^{(n)}(0)$. Low frequency moments describe the long time evolution of $M(t)$ and are $\mu_{-n} = 1/(n-1)!\int_0^\infty dt\, t^{n-1}M(t)$, i.e., $\mu_{-n} = (-1)^{n-1}/(n-1)!\ \hat{M}^{(n-1)}(0)$, where $\hat{M}(s)$ denotes the Laplace transform of $M(t)$. When a biexponential approximation $M(t) \approx f_1 \exp(-t\Gamma_1) + f_2 \exp(-t\Gamma_2)$ is applied which reproduces 2 high- and 2 low-frequency moments the coefficients and rates are

determined from $f_1\Gamma_1^m + f_2\Gamma_2^m = \mu_m$ with $-2 \le m \le 1$. These moments are

$$\mu_1 = 0, \quad [27]$$

$$\mu_0 = 1, \quad [28]$$

$$\mu_{-1} = \frac{(1 + RBV)\tau}{\sqrt{1 + (\tau\delta\omega RBV)^2} - 1 + RBV(\sqrt{1 + (\tau\delta\omega)^2} - 1)}, \quad [29]$$

$$\mu_{-2} = \mu_{-1}^2 \cdot (1 - \kappa), \quad [30]$$

with $\kappa = 1 - (1 + \mathrm{RBV})^{-1} \cdot ([1 + (\tau\delta\omega\mathrm{RBV})^2]^{-1/2} + \mathrm{RBV}\,[1 + (\tau\delta\omega)^2]^{-1/2})$. Equation [27] follows from Eqs. [3] and [4], Eq. [28] from normalization of magnetization ($M(0) = 1$). The parameters of the bi-exponential approximation are then obtained as

$$\Gamma_{1,2} = \frac{\mu_{-1} \pm \sqrt{\mu_{-1}^2 - 4\mu_{-1}^2\kappa}}{2\mu_{-1}^2\kappa}$$

$$= \mu_{-1}^{-1}\frac{1 \pm \sqrt{1 - 4\kappa}}{2\kappa} \quad [31]$$

$$f_{1,2} = \pm\Gamma_{2,1} \cdot (-\mu_{-1})\frac{\kappa}{\sqrt{1 - 4\kappa}}$$

$$= \frac{1}{2}\left(1 \mp \frac{1}{\sqrt{1 - 4\kappa}}\right) \quad [32]$$

REFERENCES

1. Bauer WR, Nadler W, Bock M, Schad LR, Wacker C, Hartlep A, Ertl G. Theory of the BOLD effect in the capillary region: an analytical approach for the determination of T_2* in the capillary network of myocardium. Magn Res Med 1999;41:51–62.
2. Kennan RP, Zhong J, Gore JC. Intravascular susceptibility contrast mechanisms in tissues. Magn Res Med 1994;31:9–21.
3. Atalay MK, Reeder SB, Zerhouni EA, Forder JR. Blood oxygenation dependence of T_1 and T_2 in the isolated, perfused rabbit heart at 4.7 T. Magn Res Med 1995;34:623–627.
4. Li D, Dhawale P, Rubin PJ, Haacke EM, Gropler RJ. Myocardial signal response to dipyridamol and dobutamin: demonstration of the BOLD effect using a double-echo sequence. Magn Res Med 1996;36:16–20.
5. Wacker CM, Bock M, Hartlep AW, Beck G, van Kaick G, Ertl G, Bauer WR, Schad LR. Changes in myocardial oxygenation and perfusion under pharmacological stress with dipyridaomole: assessment using T_2* and T_1 measurements. Magn Reson Med 1999;41:686–695.
6. Kaul S, Jayaweera AR. Coronary and myocardial blood volumes (editorial). Circulation 1997;96:719–724.
7. Donahue KM, Burstein D, Mannings WJ, Gray ML. Studies of Gd-DTPA relaxivity and proton exchange rates in tissue. Magn Res Med 1994;32:66–76.
8. Chrystal GJ, Downey HF, Bashour FA. Small vessel and total coronary blood volume during adenosine infusion. Am J Physiol 1981;241 (Heart. Circ. Physiol. 10):H194–H201.
9. Dattagupta S, Blume M. Stochastic theory of line shape I. Nonsecular effects in the strong collision model. Phys Rev B 1974;10:4540–4550.
10. Bauer WR, Schulten K. Nuclear spin dynamics (I = ½) under the influence of random perturbation fields in the strong collision approximation. Ber Bunsenges Phys Chem 1992;96:721–723.
11. Nadler W, Schulten K. Generalized moment expansion for Brownian relaxation processes. J Chem Phys 1985;82:151–160.
12. Atalay MK, Forder JR, Chacko VP, Kawamoto S, Zerhouni EA. Oxygenation in the rabbit myocardium: assessment with susceptibility dependent MR imaging. Radiology 1993;189:759–764.
13. Bassingwaighte JB, Ypintsol T, Harvey RB. Microvasculature of the dog left ventricular myocadium. Microvascular Res 1974;7:229–249.
14. Kiselev VG, Posse S. Analytical theory of susceptibility induced NMR signal dephasing in a cerebrovascular network. Phys Rev Lett 1998;81(25):5696–5699.
15. Kiselev VG, Posse S. Analytical model of susceptibility induced MR signal dephasing: effect of diffusion in a microvascular network. Magn Res Med 1999;41(3):499–501.
16. Boxerman JL, Hamberg LM, Rosen BB, Weisskoff RM. MR contrast due to intravascular magnetic susceptibility perturbations. Magn Res Med 1995;34:555–566.